THE NUMERICAL ANALYSIS OF DAMAGE IN TEXTILE COMPOSITES USING A MULTI-SCALE APPROACH

P.R. Cunningham*, P. Römelt

Department of Aeronautical and Automotive Engineering, School of Aeronautical, Automotive, Chemical and Materials Engineering, Loughborough University, Leicestershire LE11 3TU, UK.

**p.cunningham@lboro.ac.uk*

Keywords: Textile composites, multi-scale modelling, damage.

Abstract.
A numerical analysis procedure based on a multi-scale finite element (FE) approach for modelling damage in textile composites is presented in this paper. The approach uses a meso-scale full FE model of a unit cell to determine the input parameters for an equivalent binary unit cell model [1], which is then used to build a macro-scale model of the complete specimen. Results from the numerical analysis are compared with experimental stress-strain data for a specimen tested to failure. The results compared favourably throughout the test range, with excellent agreement in the lower strain range, and a deviation of 6% for larger strains.

1 Introduction.

The numerical analysis of damage initiation and propagation in textile composites requires models which take into account the different modes of failure, such as tow-matrix de-bonding and crack propagation within the tows and matrix. Multi-scale modelling offers many advantages when applied to woven composite structures, particularly in terms of capturing the overall effect of these damage events which are often best observed on the meso-scale. This suggests that a multi-scale approach which uses meso-scale models to generate material input parameters for macro cells would be the most suitable method to model the behaviour of a woven macro-structure subject to the initiation and propagation of damage.

Three different and distinct approaches to numerically model woven macro-structures can be found in the literature; the full finite element approach [2], the voxel technique [3] and the binary model [1]. For the full finite element approach, precise geometrical data is required to generate a reasonably accurate model of a unit cell comprising a repeating pattern of the woven structure. These models allow the stress distribution within the unit cell to be determined to a high resolution, depending on the element density. Lomov et al. have shown that this method has been used successfully to predict damage initiation [4]. The main disadvantages of full finite element modelling are the complexity of the model and high number of elements required to provide realistic estimates of the stress distribution. The voxel technique uses sub-meso volumes that are created by overlaying a two-dimensional grid over the top of a geometrical unit cell and computing the average material properties which are dependent on the through thickness architecture [5]. These material properties are then

assigned to three dimensional elements generated at the two dimensional grid point positions. The method results in a reduction in the effort required to mesh the model, however the resulting stress distribution is averaged out over the model, which means that stress concentrations are averaged out making it difficult to reliably estimate damage initiation sites. Finally, the binary model was established by Cox and Yang [1] and utilizes one-dimensional elements to represent the tows of the woven architecture. The one-dimensional elements represent the axial properties of the tows, whereas the remaining composite properties are represented using three-dimensional "effective medium elements". As with the voxel technique, the binary model reduces meshing effort and computational cost while averaging out stress concentrations.

In this paper, a multi-scale approach is used to model the damage initiation and propagation in a textile composite. A meso-scale full finite-element approach is used to verify the damage initiation locations and propagation and to further generate the non-linear input parameters for an equivalent binary model, which is then used to model the composite structure on the macro-scale.

2 Specimen manufacture, analysis and testing.

Prior to the development of the numerical models, suitable experimental test specimens were manufactured, analysed and tested in order to obtain the data for the weave geometry necessary to develop the full finite element model, and the stress-strain data which will be used to compare with the results of the numerical analysis. The material used in this investigation was Gurit RE86P plain weave E-glass fabric together with Gurit Prime 20LV epoxy resin for the matrix. The material properties for these constituents were obtained from the manufacturer's data sheets together with the Matweb database, and are summarized in table 1. A 2.5mm thick plate of dimensions 330mm × 330mm was manufactured by infusing thirty plain weave layers with the epoxy resin using a double bag vacuum infusion procedure [6]. The specimens for the microscopic analysis and the tensile test specimens were cut from this laminated plate.

E-glass fibre properties		**Epoxy resin properties**	
E [GPa]	72.4	E [GPa]	3.5
G [GPa]	30.0	G [GPa]	1.3
ν [-]	0.2	ν [-]	0.35
		σ_{ult} [MPa]	73
		τ_{ult} [MPa]	137
		K_{IC} [MPa(m)$^{0.5}$]	3.7

Table 1. Material properties for the E-glass fibre and Gurit Prime 20LV epoxy resin used in the manufacture of the test specimens.

2.1 Microscopic analysis of the laminated textile composite.

The microscopic specimens were cut from the laminated plate at various locations and were cast in a dyed epoxy resin to provide contrast when viewed under the microscope. The specimens were polished using a five-step process and digital images were taken at 20-times magnification for the tow path analysis and 80-times magnification for tow cross-section analysis. A typical image at 80-times magnification from the microscopic analysis is shown in figure 1. These images were used to obtain average tow path and cross-section parameters to be used in the numerical models, with a sine fit used for the tow path parameters, and an elliptical fit used for the cross-section parameters. The results from an analysis of over one hundred images are given in table 2 and further details can be found in [7].

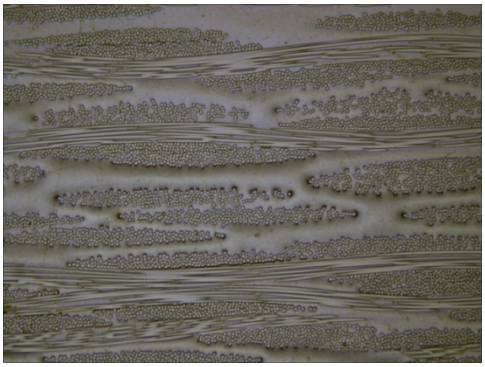

Figure 1. A typical microscopic image of the E-glass / epoxy textile composite specimens showing tow path and cross-section (80-times magnification).

Parameter [unit]	Average value ± standard deviation
Tow path amplitude [mm]	0.025±0.009
Tow path ½ wavelength [mm]	1.604±0.164
Tow cross section major axis [mm]	0.187±0.066
Tow cross-section minor axis [mm]	0.037±0.007
Tow cross-sectional area [mm^2]	0.022

Table 2. Average geometrical properties of the woven textile meso-structure.

2.2 Tensile tests

The tensile test specimens were cut from the laminated plate with a $[0/90]_{30}$ configuration. A 120Ω rectangular rosette strain gauge with a 5mm gauge length was bonded to each of the nine specimens, and tensile tests were conducted according to ASTM D3039. The results from the tensile tests using nine test specimens are shown in figure 2, with the mean stress-strain curve shown on the graph. The average variation in the curves is 7% about the mean, with failure strengths ranging from 375MPa to 450MPa giving a +9.8% to -8.5% variation at failure. The variation in the results is consistent with those reported by Daggumati et al [8].

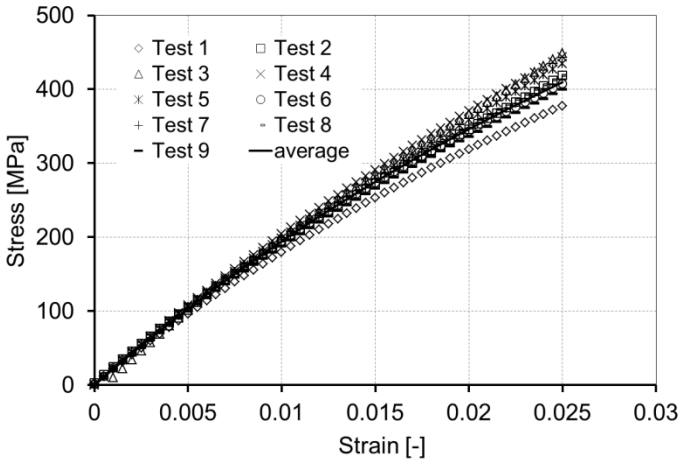

Figure 2. Tensile test results.

3 Development of the numerical models.

The numerical models were developed using PATRAN as the pre-processor to model the geometry and for meshing, with ABAQUS/Standard and ABAQUS/CAE used as the solver and post-processor respectively.

3.1 Meso-scale full finite element unit cell model.

The parameters given in table 2 were used to define the geometry of the tows in the full finite element unit cell model. Eight-node brick elements were used to generate the mesh which had a total of 117,096 degrees of freedom. The woven architectures being modelled in this paper have highly elliptical cross-sections, as evident from figure 1. It is therefore a challenge to generate a full finite element unit cell model with enough refinement and with the minimum number of elements with high aspect ratios and skew angles. For the mesh in this paper, only 3% of the elements had an aspect ratio greater than the recommended value of 5 or skew angles greater than 30%, which was deemed an acceptable level for a model of this type [9]. The full finite element unit cell mesh is shown in figure 3.

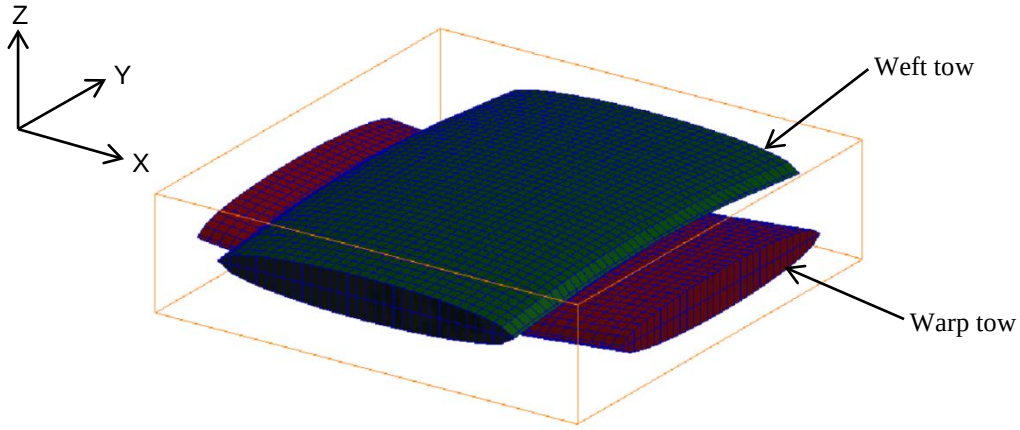

Figure 3. Full finite element unit cell mesh (the matrix mesh has been omitted for clarity).

The boundary conditions for this meso-scale model were assumed to be periodic [10]. A constant displacement was applied to all of the nodes on the y-z faces of the unit cell in the axial direction, and on the x-y and x-z faces the nodes were kept straight to allow for Poisson's effect. The centre node of the unit cell model was constrained in both y and z to prevent rigid body motion in these directions.

3.1.1 Damage initiation and propagation.

Cohesive elements with a traction-separation formulation [11] were used to model damage initiation, propagation, and tow-matrix de-bonding in the full finite element unit cell model. In order to determine the optimum location for the cohesive elements, a linear analysis was conducted with the model to locate the areas of stress concentration, which were near the edge of the weft tows and at the edge of the tow/matrix interface [7]. These results were consistent with similar studies found in the literature [8, 12]. A maximum traction criterion was used in conjunction with a damage variable to simulate the damage initiation and propagation in the cohesive elements, which was an option within ABAQUS/Standard. The damage variable is calculated based on the combined effect of normal and shear tractions within the element. Figure 4 shows the value of the damage parameter at two global tensile strain levels for the full finite element unit cell model including cohesive elements. These results show how the damage is estimated to propagate within the unit cell, with initiation between the weft tow and the matrix at the point of highest stress concentration, and propagation into the weft tow and the matrix. On one side of the tow, the damage spans the whole width of the tow, while on the other side the damage extends to half the width of the tow, which was also observed by Gao et al. for a 8-harness satin weave laminate [12]. The damage progresses as tow matrix interface failure within the numerical model and the matrix between the warp and weft tows is unloaded. Tow/matrix de-bonding was also observed in the numerical model, which was also consistent with findings from experimental tests in the literature [8, 12].

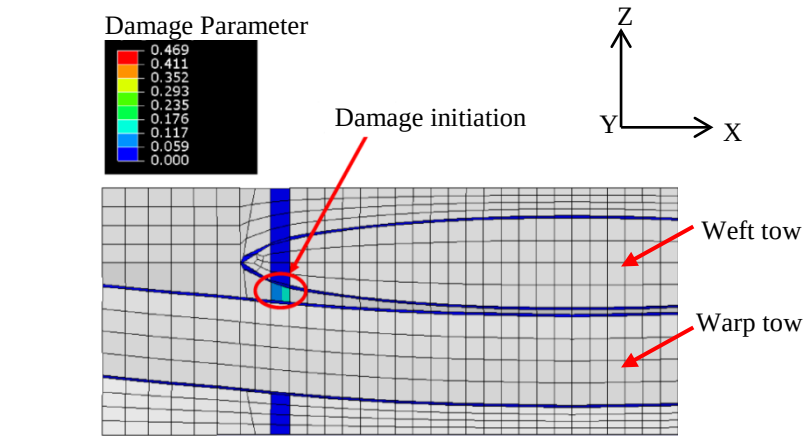

(a) 0.37% global tensile

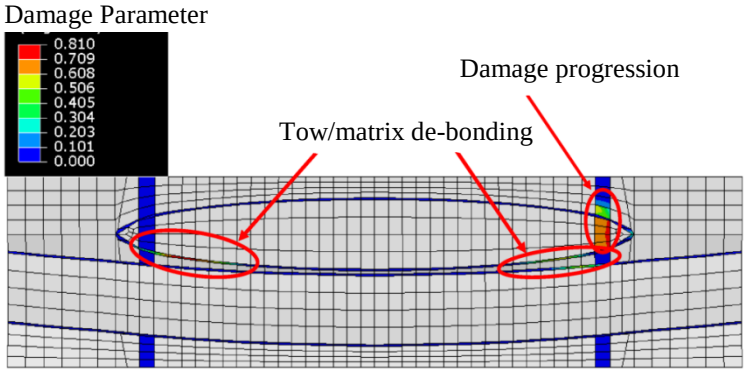

(b) 0.75% global tensile

Figure 4. Damage parameter for the full finite element unit cell model at two global tensile strain values.

3.2 Binary unit cell model.

For the binary unit cell model [1], three dimensional hex-elements were used to model transverse tow and surrounding matrix properties, and the axial stiffness of the tows was modelled using one-dimensional spring elements embedded in the three-dimensional mesh. The mesh geometry and element properties, namely the location and spring stiffness for the one-dimensional elements and the linear isotropic material properties for the three-dimensional elements, were calculated using the tow geometric parameters obtained from the microscopic analysis and the rule of mixtures for an equivalent unidirectional laminate with a fibre volume fraction comparable to the multi-axial composite.

3.2.1 Damage modelling using non-linear spring elements.

The model in this paper differs from that of Cox and Yang [1] in that non-linear one-dimensional spring elements were used in order to capture the overall damage initiation and propagation within the unit cell. The complete load-displacement history from the full finite element unit cell model was used to calculate the input parameters to the one-dimensional spring elements by using the tangent modulus derived from the true stress-strain curve. The one dimensional elements and three dimensional elements were modelled as a series of springs, as shown in figure 5. For each three-dimensional element, four one-dimensional spring elements were used to reproduce the tow path and therefore model the axial stiffness of the tow. Due to tow crimp the local orientation of the one-dimensional spring elements is not in the axial direction of the element, so the stiffness of each spring element needs to be corrected by using the scalar product of the normalized local tow path tangent vector **t** with the global axial unit vector $\mathbf{e}_x$ as shown in equation 1.

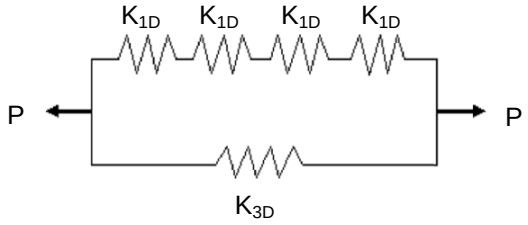

Figure 5. Binary model non-linear spring stiffness modeling approach.

$$K_{1D} = K_{spring} \sum_{i=1}^{4} \frac{\mathbf{t_i}}{|\mathbf{t_i}|} . \mathbf{e_x} \tag{1}$$

where

$$K_{spring} = (E_t - E_{3D}) \frac{A}{L} \tag{2}$$

and E_t is the transverse Youngs modulus of the tow, E_{3D} is the Young's modulus of the matrix, and A and L are the cross-sectional area and length of the equivalent binary unit cell respectively. The force-displacement relationship of this equivalent binary unit cell was verified by comparing a model consisting of eight binary blocks, to give the equivalent boundary conditions, with the results from the full finite element model. The binary model is shown in figure 6.

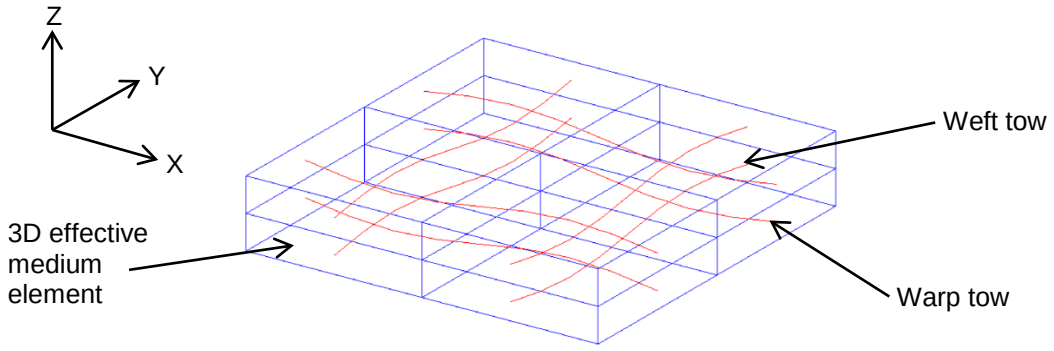

Figure 6. Eight-block equivalent binary unit cell model used to verify the force-displacement relationship.

Finally, a macro-scale model consisting of nine binary blocks width-wise and in the axial direction and thirty blocks stacked in the thickness direction was developed to represent the critical cross section of the tensile test specimen. The model had a total of 540,186 degrees of freedom for the macro-scale model of a representative structure. Boundary conditions were chosen to best represent the conditions at the cross-section of the test specimen. A uniform displacement was applied to the y-z faces of the model and the centre node of the model was fixed in both the y and z direction to constrain rigid body motion. Rotation around the x-axis was constrained by fixing the translation of the two nodes in the centre of the x-z faces in the z-direction.

4 Discussion of results

4.1 Comparison of the full finite element and equivalent binary unit cell models.

The stress-strain response of the equivalent binary unit cell model is compared with the full finite element unit cell model in figure 7. There is a good agreement between the two models, verifying the approach taken in developing the equivalent binary unit cell model. The deviation in stress at 2.5% strain is 4%, which could be attributed to the non-linear force-

displacement input parameter obtained from the full finite element model. The spring stiffness, derived from the slope of the force displacement curve, was constant after 0.5% strain [7]. The damage in the full finite element model initiated as a weft yarn/matrix interface failure and propagated to the boundary of the unit cell, whereby load was carried by the tow only which was assumed to be linear-elastic in the model, hence the constant slope.

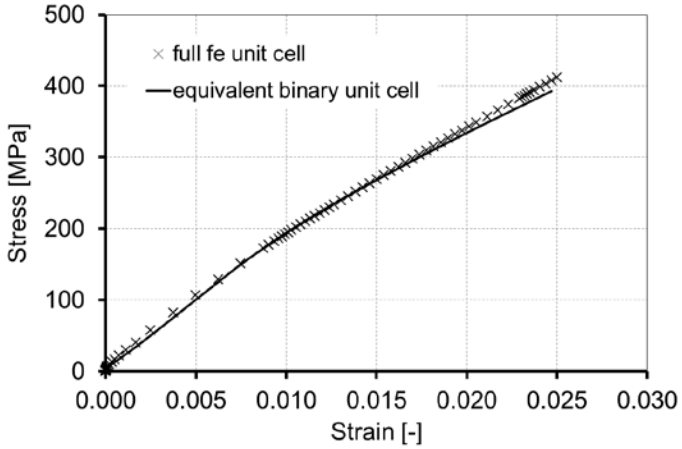

Figure 7. Comparison of the full finite element and equivalent binary unit cell models.

4.2 Macro-scale model results.

The result from the macro-scale model compared with the tensile test specimen result is shown in figure 8. The agreement between the numerical macro-scale model and the experimental result is very good, particularly for strains up to 1.5%. For higher strain levels, there is a progressive deviation between the two results up to an average of 6% at maximum 2.5% strain. The macro-scale model result does however stay within the experimental bounds.

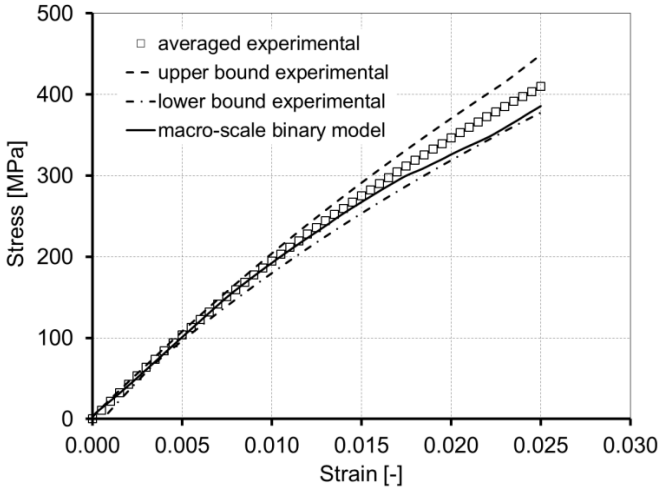

Figure 8. Comparison of the macro-scale binary model and the experimental stress-strain results.

There are several limitations of the model which could be attributed to the discrepancies observed. Firstly, the damage that was modelled within the full finite element unit cell and subsequently used as a non-linear input parameter to the equivalent binary unit cell model cannot progress beyond the bounds of the unit cell. On the macro-scale, this damage progression is therefore not truly representative of the events that must be taking place within the experimental test. In addition, the mechanical behaviour of both constituents within the

full finite element numerical model are assumed to be linear-elastic with a linear degradation of the selected matrix elements. In practice, E-glass fibre tows exhibit strain dependent material properties, and epoxies behave visco-elastically. These features were not incorporated in the numerical models at this stage.

5 Conclusions

A procedure to numerically model the macro-behaviour of woven textile composites is presented in this paper. A full finite element meso-scale model with cohesive elements was used to model the damage initiation and propagation within the unit cell, and the resulting non-linear force displacement relationship was used as an input parameter to an equivalent binary unit cell model using one-dimensional elements to represent the tows. A comparison between a macro-scale model of a test structure consisting of an arrangement of binary unit cells was compared with average tensile stress-strain experimental results, and good agreement was obtained up to 1.5% strain. A deviation of 6% was found at higher strain levels, which could be attributed to the limitations of modelling damage growth beyond the unit cell and the use of linear mechanical properties of the constituent materials.

References

[1] Cox B.N., Yang, Q. Predicting failure in textile composites using the binary model with gauge averaging. *Eng. Fract. Mech.*, **77**, pp. 3174-89 (2010).

[2] Tserpes, K.I., Labeas, G., Pantelakis, S. Multi-scale modeling of the mechanical response of plain weave composites and cellular solids. *Theor. Appl. Fract. Mech.* **54**, pp. 172-79 (2010).

[3] Bogdanovich, A.E. Multi-scale modeling, stress and failure analysis of 3-D woven composites. *J Mater. Sci.* **41**, pp. 6547-90 (2006).

[4] Lomov, S., Ivanov, D.S., Verpoest, I. et al. Meso-FE modeling of textile composites: road map, data flow and algorithms. *Compos. Sci. Technol.* **67**, pp. 1870-91 (2007).

[5] Crookston, J.J., Ruijter, W., Long, A.C., Jones, I.A. *Modelling mechanical performance including damage development for textile composites using a grid-based finite element method with adaptive mesh refinement* in "Proceedings of *8th International Conference on Textile Composites (TEXCOMP-8)*", Nottingham, UK, (2006).

[6] Williams, C. Summerscales, J. Grove, S. Resin infusion under flexible tooling (RIFT): a review. *Composites Part A.* **27**, pp. 517-24 (1996).

[7] Romelt, P., Cunningham, P.R. A multi-scale finite element approach for modeling damage progression in woven composite structures. *Composite Structures.* **94**, pp. 977-89 (2012).

[8] Daggumati, S., De Baere, I., Van Paepegem, W. et al. Local damage in a 5-harnes satin weave composite under static tension: part I – experimental analysis. *Compos. Sci. Technol.* **70**, pp. 1926-33 (2010).

[9] Glaessgen, E.H., Pastore, C.M. et al. Geometrical and finite element modeling of textile composites. *Composites Part B.* **27**, pp. 43-50 (1996).

[10] Whitcomb, J.D., Chapman, C.D., Tang, X. Derivation of boundary conditions for micromechanics analyses of plain and satin weave composites. *J. Compos. Mater.* **34**, pp. 724-47 (2000).

[11] Ridha, M., Tan, V.B.C., Tay, T.E. Traction-separation laws for progressive failure of bonded scarf repair of composite panel. *Compos. Struct.* **93**, pp. 1239-45 (2011).

[12] Gao, F., Boniface, L., Ogin, S.L. et al. Damage accumulation in woven-fabric CFRP laminates under tensile loading: Part 1: Observations of damage accumulation. *Compos. Sci. Technol.* **59**, pp. 123-36 (1999).